Nucleation and Mesostrain Influence on Percolating Critical Currents of Solution Derived $YBa_2Cu_3O_7$ Superconducting Thin Films

X.Obradors[1*], F. Martínez-Julián[1], K. Zalamova[1], V.R. Vlad[1], A.Pomar[1], A. Palau[1], A. Llordés[1], H. Chen[1], M. Coll[1], S. Ricart[1], N. Mestres[1], X. Granados[1], T. Puig[1], M. Rikel[2]

(1) Institut de Ciència de Materials de Barcelona (ICMAB-CSIC), Campus Universitat Autònoma de Barcelona, 08193 Bellaterra, Spain

(2) Nexans Superconductors, 50354 Hürth, Germany

* Xavier.obradors@icmab.es

Abstract **- After briefly reviewing the present understanding of the nucleation process of YBCO films, a new approach is presented to enhance the stability of c-axis nucleation in epitaxial chemical solution deposited YBCO thin films derived from TFA precursors. We show that with silver addition to the TFA precursor c-axis nucleation can be reached in a wide range of temperature thus keeping high percolating J_c. We argue that silver reduces supersaturation and makes more stable the c-axis nuclei without modifying T_c. Additional advantages of silver addition are an enhanced surface smoothness and a reduced porosity of the YBCO films. The second reported topic relates to the discovery of an adverse relationship between percolating J_c and YBCO films mesostrain, as determined through X-ray diffraction line broadening. We show that mesostrain is enhanced in processes leading to inefficient strain healing at grain boundaries, for instance annealing times too short or growth temperatures too low. It is suggested that the strained regions at the low angle grain boundaries lead to a weak link behavior which can be microscopically understood on the basis of pair formation prevention, as proposed by the bond contraction pairing model.**

Preprint of invited SCC paper submitted to *Physica C* (should be cited accordingly)
Submitted to ESNF November 30, 2011; accepted Dec. 23, 2011. Reference No. ST292; Category 2.

Keywords **– HTS, YBCO, thin films, chemical solution deposition, nucleation, grain boundaries, mesoscopic strain, critical currents**

I. INTRODUCTION

Achieving high critical current in high temperature superconducting (HTS) wires has been a very significant objective of research during recent years. High quality biaxially textured conductors (coated conductors, CC's) has been developed which helped to overcome the main factor limiting the performance of CC's grain boundaries.

In the last years considerable effort has been devoted to understand the mechanisms controlling epitaxial growth and grain boundary structure of superconducting thin films based either on vacuum-deposited or low-cost chemical solution deposition (CSD) methods in order to boost their use in coated conductors technology [1-3]. The so-called trifluoroacetates (TFA) route has been up to now the most successful CSD approach [4-6]. Briefly, a precursor solution of Y, Ba and Cu trifluoroacetates or other metallorganic salts is deposited on the substrate by an adequate technique such as spin, dip or web coating, ink jet deposition) [2, 3, 7] leading to uniform and controlled thickness. Then, the precursor solution is heat treated to from YBCO thin films previous formation of solid nanocrystalline intermediate phases, one of them being BaF_2. This CSD ex-situ growth process bears many similarities, and some discrepancies, to physical vapor deposition (PVD) techniques of Y and Cu metals together with BaF_2 [1-3, 8, 9]. This is because the intermediate process steps in CSD films, i.e. solution deposition, metallorganic pyrolysis and solid precursors phase transformations have a complex interplay into the final YBCO film microstructure and superconducting performances which still remain controversial in many aspects [2, 3, 5, 10-12]. More precisely, the knowledge of the influence of the different reaction parameters (temperature, gas flow, partial water pressure, oxygen pressure, ...) on the film epitaxial quality and superconducting properties remain still poor [5, 10, 12]. One essential issue has been proven to be avoiding the undesired formation of randomly oriented or a/b-axis grains which introduce high angle grain boundaries and very often enhance the film porosity. Hence understanding how the nucleation process proceeds has a top priority. [13-21].

It is now understood that ex-situ growth process is characterized by a Volmer – Weber heterogeneous nucleation mechanism where islands are formed at the interface with the substrate, and then the grains grow until coalescence forming finally a continuous film. Stringent efforts have been made to understand the grain boundary

(GB) structure resulting from this ex-situ process in order to achieve high percolating critical current densities J_c [22-25], however many details relating the GB structure with the critical currents remain elusive [26, 27]. A new view of this problem has been recently proposed: It has been suggested that the tensile strain associated with the dislocations located along GB's lies at the origin of the universal weak link behavior observed in HTS and pnictides and keeping some parallelism to the modified mesoscale magnetism at grain boundaries in colossal magnetoresistive films [28, 29].

In this work we will first review the nucleation process of YBCO films and then we will report about two new contributions for achieving an enhanced control of microstructure and self-field critical currents in YBCO films grown by CSD. First, we will show that by adding silver to the YBCO-TFA solution we can enhance the c-axis nucleation and hence extend the temperature window where epitaxial films can be obtained. A second advancement reported in this work arises from an experimental analysis of the inhomogeneous strain at grain boundaries (mesostrain) which influences adversely the percolating critical currents. We will show that during the zipping process, following the island coalescence, the mesostrain accumulated at the GB is healed out and this increases the percolating critical current density of the films.

II. EXPERIMENTAL

The YBCO films used in this work were prepared by the trifluoroacetates route as described in detail previously [2] by using anhydrous precursor solutions with 1.5 M concentration [30]. Silver trifluoroacetate in molar proportions ranging from 2.5 mole % to 20 % mole were added when indicated. Gel films formed after dip or spin coating followed a fast pyrolysis (~ 30 min) process at 310ºC in oxygen atmosphere while growth was performed with different annealing times at temperatures between 720ºC and 810ºC. Normal pressure conditions (P_t=1 bar), PO_2 = 0.2 mbar and P_{H2O} = 23 mbar were used; linear gas flow velocity of 26 10^{-3} m/s. The heating ramp to reach the reaction temperature was of 1500ºC/h. The substrates were YSZ single crystals buffered with PVD-CeO_2 (100 nm) supplied by THEVA GmbH or with CSD-$Ce_{0.9}Zr_{0.1}O_2$ (CZO/YSZ) or $LaAlO_3$ (LAO) single crystals. The YBCO film thickness was 250±20 nm, as determined by profilometry.

Structural characterization of films fully processed (additionally annealed for 2 h in 100% O_2 at 450-500°C) or just quenched after annealing at 770ºC was made using x-ray

diffractometer equipped with a 2D detector (GADDS-Bruker). Conventional θ-2θ patterns were recorded to determine the microstrain using the Williamson – Hall (WH) plot after correction for the instrumental width of Bragg peaks. Out-of-plane (Δω) and in-plane (Δϕ) grain misorientation were those typical of single crystalline substrates (~0.5º and ~1º, respectively). FE-SEM and atomic force microscopy in the tapping mode (AFM) images were also obtained to visualize the surface morphology of the films which confirmed typical flat-like grain morphologies. Critical current densities of the YBCO films were measured inductively with a SQUID magnetometer up to applied fields of 7T while T_c was found inductively to be in the range of 90-91 K. Both percolating J_c^{PERC} and intragrain J_c^{G} critical currents were determined simultaneously in some cases following a method recently proposed by Palau et al [31, 32]. For some samples, the YBCO film growth was monitored by in-situ electrical resistance measurements using a DC 4-probe method following the procedure recently described by Chen et al [13].

III. NUCLEATION IN YBCO THIN FILMS

It was early discovered that YBCO thin films grown by whatever in-situ or ex-situ technique have specific regions of the PO_2-T phase diagram where c-axis nucleation and growth is optimal while at reduced temperatures and PO_2 values a coexistence of c-axis and a-axis orientations is observed [33]. The origin of such a behavior has been not yet clearly established and while early assessments attributed this to kinetic effects, more recent analysis suggest that it has a thermodynamic origin and classical nucleation theory can essentially cope with it.

Ex-situ grown YBCO films have been shown to nucleate following a Volmer – Weber mode, i.e. single islands are first formed in random positions of the interface with the substrate and then grow along all directions, at different growth rates, and finally coalesce leading to a continuous film [9, 34, 35]. However, some systems display a complex growth behavior, such as REBCO (RE= Rare Earth) or CeO_2 [36-38], because the formation energies of diverse crystal orientations are very close and so they can be formed simultaneously. A thermodynamic analysis of the parameters influencing the nucleating event is thus required to achieve a tight control of the final microstructure of the films [39].

YBCO oxide can nucleate with the *c*-axis either perpendicular to the substrate ((00l) plane parallel to the substrate, c-axis nuclei) or parallel to it (i.e., (100) plane parallel to the substrate, a-axis nuclei), depending on several parameters such as temperature, $P(O_2)$, lattice misfit with the substrate, RE ion, etc. [38, 40-46]. A crossover temperature exists where the most stable crystalline orientation during the nucleation process changes from one type to another. This may happen because the free energies of two crystalline orientations have a different dependence on the nuclei size. In this way, when the supersaturation conditions are modified the critical size of the first stable nuclei also change and, eventually, the most stable island orientation is controlled [38, 44]. This issue has often not been taken into account and oversimplified scenarios were suggested. Classical nucleation theory states that the stability of the first nuclei is controlled by the Gibbs energy barrier ΔG^* to form islands and so the energy of an isolated interfacial island needs to be computed. In general the energy of an epitaxial island has a term determined by the surface and interface energy contributions E_{surf} and a second term E_{relax} arising from the relaxation of the elastic energy associated with the lattice misfit between the nucleus and the substrate [39, 47]. At the nucleation stage, however, the second term can be neglected due to the small size of the first stable nuclei. Therefore we can compute the Gibbs energy barrier ΔG^*, if we assume a cylindrical shape for the interfacial epitaxial grains with height h and radius r [38, 44]. The total Gibbs change during YBCO crystallization can be written as

$$\Delta G(r) = \frac{\pi h r^2}{v}\Delta\mu + 2\pi h r\gamma_{lat} + \pi r^2(\gamma_{up} + \gamma_{int} - \gamma_{sub}) \quad (1)$$

where v and γ represent the unit cell volume and surface free energy per unit area (lat = lateral surface, up = upper surface, int = interface, sub = substrate), $\Delta\mu$ (<0) is the chemical potential change per molecule between the epitaxial YBCO phase and the precursor random nanocrystalline state. The energy barrier for heterogeneous nucleation ΔG^*, corresponding to the critical nuclei radius $r^* \propto (-1/\Delta\mu)$, can be deduced by maximizing ΔG^* vs. r in eq. (1), i.e. $(\partial \Delta G(r)/\partial r = 0)$, which leads to the following result,

$$\Delta G^* = \frac{\pi(h\gamma_{lat})^2}{-\left(\frac{h}{v}\right)\Delta\mu - (\gamma_{up} + \gamma_{int} - \gamma_{sub})} \quad (2)$$

This energy barrier has been found to be different for YBCO nuclei with different orientations and so the dependence of ΔG* on Δμ can be calculated for the corresponding combination of surface energies (Figure 1). As can be seen from Fig. 1, it is predicted that c-axis grains nucleate under low supersaturation conditions (low $|\Delta\mu|$), while a-axis and c-axis nucleation can have similar rates under high supersaturation conditions (large $|\Delta\mu|$) because the corresponding energy barriers $\Delta G^*(001)$ and $\Delta G^*(100)$ are very similar [38, 40-42].

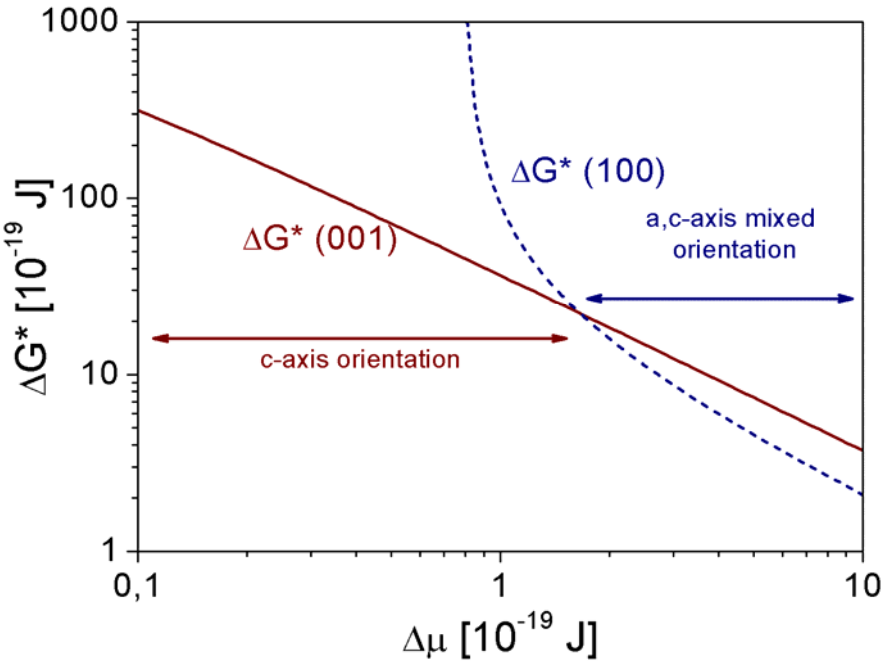

Fig. 1. Typical dependence of nucleation energy barriers ΔG* with the chemical potential change in YBCO growth. The dependence of the (00l) and (100) nuclei are indicated [40].

In ex-situ growth of TFA-YBCO films the proper chemical conversion reaction is the following [11, 13]:

$$Ba(O_xF_y)_2 + \frac{3}{2}CuO + \frac{1}{4}Y_2O_3 + yH_2O \rightarrow \frac{1}{2}YBa_2Cu_3O_{6.5} + 2yHF \qquad (3)$$

The chemical potential change associated to this reaction can be written as follows [17, 21, 34]:

$$\Delta\mu = \Delta\mu_0 + y\mathrm{k}T\ln\left(P_{\mathrm{HF}}^2 / P_{\mathrm{H_2O}}\right) \tag{4}$$

where $\Delta\mu_o = \Delta h_o - T\Delta \mathrm{s}_o$, Δh_o and Δs_o are respectively the enthalpy (heat of sublimation) and entropy change of the formation reaction (between the epitaxial YBCO phase and the precursor random nanocrystalline state); P_{HF} and $P_{\mathrm{H_2O}}$ are HF and H_2O partial pressures in the vicinity of the YBCO nucleus sites. We should note that both terms in this equation have a negative sign and that when in-situ growth techniques are used only the first term of eq. (4) needs to be considered.

The statistical process of overcoming the energy barrier leads to a nucleation rate dN/dt given by

$$\frac{dN}{dt} = \frac{dN_0}{dt}\exp(-\Delta G^* / kT) \tag{5}$$

where N is the number of stable nuclei on the substrate surface per unit area, t is time and dN_0/dt is the nucleation rate with a negligible nucleation barrier, $\Delta G^* \approx 0$.

The kinetics of nuclei formation in any process will be then determined by a particular time integration of eq. (5). Very few detailed analysis have been performed, however, of the complex issue of quantifying the nucleation density in relationship with well defined substrate characteristics and processing conditions [16-18, 34, 38, 40]. It has been suggested, for instance, that the grain size in vicinal CeO_2 cap layers can strongly influence the YBCO nucleation rate [48] while we have shown that enhanced CeO_2 surface planarities lead to larger percolating critical currents [49, 50].

A certain consensus concerning the influence of diverse parameters in the nucleation process of in-situ and ex-situ grown films has been reached which is summarized in Table I.

Table I – Trends concerning the influence of processing parameters on the nucleation crossover from (00l) to (100) crystalline orientations in REBCO thin films grown by in-situ or ex-situ (P_T=1 bar un less indicated otherwise) methodologies.

Parameter evolution	**In-situ growth**	**Ex-situ growth**
T increase	c-axis nucleation enhanced	c-axis nucleation enhanced
PO_2 increase	Multiple nucleation enhanced	Multiple nucleation enhanced
PH_2O increase	No influence	Multiple nucleation enhanced
P_T decrease	No influence	Multiple nucleation enhanced
Gas flow increase	No influence	c-axis nucleation enhanced
RE atomic number increase	c-axis nucleation enhanced	c-axis nucleation enhanced

The temperature dependence of /Δμ/ and hence of the energy barriers ΔG* corresponding to (00l) and (100) orientations is explicitly made evident in eq. 4 and the evolution trends have been explored for both, in-situ and ex-situ growth methodologies. Supersaturation is usually reduced when temperature is increased, thus stabilizing c-axis nuclei, for in-situ and normal total pressure, P_T, ex-situ growth [12, 18, 38, 40]. This means that under these conditions the first term in eq. (4) is dominating over the second one, an issue that can be justified after the determination of typical P_{HF} and $P_{\mathrm{H_2O}}$ values in ex-situ growth (P_{HF} = 10^{-4} bar and P_{H_2O} = 2 10^{-3} bar) [51, 52]. However, it is also clear that the degree of supersaturation in ex-situ grown films can be strongly modified by $P_{\mathrm{H_2O}}$ and P_{HF} i.e. by P_T, and this has been indeed experimentally proved [12, 18, 21]. For instance, c-axis nucleation can be achieved at lower temperatures when $P_{\mathrm{H_2O}}$ is increased or P_{HF} (and P_T) is decreased, in agreement with eq. (4). At reduced P_T values, eventually, the temperature dependence of supersaturation degree can be even reversed if the second term in eq. (4) becomes dominant over the first one and then c-axis nucleation is preferential at lower temperatures than a-axis nucleation [21]. The influence of PO_2 on the nucleation process has been investigated in less detail and in a quite narrow range of values up to now and so the trends reported in Table 1 are less

prone to quantitative estimations [12, 17, 21]. Concerning the quantitative influence of RE atomic number into the issue of the crossover between c-axis and a-axis dominated nucleation, a full phase diagram with the same amount of details than YBCO is still lacking. However, it has been suggested that, based on the experimental fact that the peritectic temperature is decreased when the RE atomic number is increased (which reduces $|\Delta\mu_0|$ in eq. (4)), a shift towards reduced temperatures of the crossover temperature occurs [40]. This fact was indeed experimentally verified in PLD-grown YbBCO thin films which can display c-axis orientation at lower temperatures than YBCO under the same growth conditions [40]. The same trend should be expected for ex-situ grown films although no experimental reports have been presented up to now.

After a controlled nucleation process, the growth rate, *R*, of ex-situ TFA-YBCO films can be determined through well specified processing conditions and values as high as *R*=1-3 nm/s can be reached [20, 21]. The solid-gas reaction leading to the formation of YBCO films following eq. (3) has been recently modeled and a single equation describes a wide range of growth conditions:

$$R = C \cdot \frac{P_{H_2O}^{1/2}}{\left(\alpha + \beta \cdot P_t + \gamma \cdot P_t / F\right)} \qquad (6)$$

where *C,* α*,* β and γ are coefficients and *F* is gas flow rate. The first three coefficients depend on temperature while γ depends on the film surface. The growth rate of YBCO films was found to be approximately independent of PO_2 [13]. The solid-gas reaction-diffusion model used in the analysis considered both the diffusion of HF gas towards the carrier gas and the chemical reaction kinetics at the growing interface. As we can see, therefore, the dependence on the processing parameters of the nucleation rate (eq. (2), (4) and (6)) and the growth rate (eq. (6)) strongly differ. As a consequence, a single set of optimal conditions for both phenomena can't exist. Therefore, achieving optimal superconducting performances with a high throughput CC production would require a double step process [13, 20].

IV. NEW APPROACH TO TUNE NUCLEATION: Ag ADDITION

Figure 2 shows the main result of this work concerning the influence of Ag additives on the performance of YBCO films. Here we present the self-field J_c at 77K of the

YBCO/Ag composite thin films with 10 % mol Ag (red and green circles) compared with that of standard YBCO films (blue squares) as a function of growth temperature.

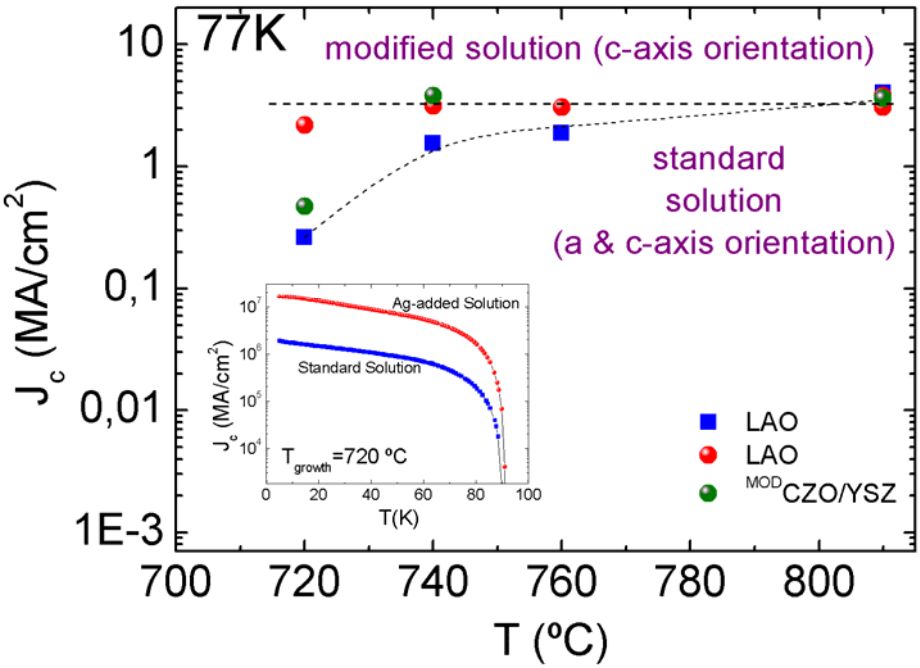

Fig. 2. Critical current density as a function of processing temperature for YBCO films prepared with Ag additive on LAO substrates (red circles) and CZO/YSZ substrates (green circles) and standard (blues squares) YBCO-TFA films. Inset: Temperature dependence of critical current for YBCO samples with and without Ag additive grown at 720ºC on LAO substrates.

TFA-YBCO/Ag films grown on LAO or ^{MOD}CZO/YSZ single crystals exhibit constant J_c values (J_c ~3 MA/cm^2) when growth temperature is kept in the range 740-810ºC. Instead, in pure YBCO films a strong decrease of J_c is observed below 760ºC. This phenomenon can be attributed to the enhanced nucleation of a/b-axis grains at low growth temperatures [4, 12, 53]. The presence of a/b-axis grains coexisting with c-axis oriented grains increases the residual porosity and enhances the density of 90º GB. The addition of these two effects tends to reduce the percolating critical current at self field [53-55]. Surprisingly, this is not the behaviour observed in the YBCO/Ag composites where J_c is almost constant for all the studied range. This is a crucial point for the fabrication of coated conductors as it will allow the use of lower reaction temperatures without degradation of performances and minimizing the interfacial chemical reactivity and the oxidation of the metallic substrates. We should note also that the presence of Ag additions in the solution has no evident influence on the critical temperatures of the

YBCO/Ag films which are similar to the pure YBCO samples (T_c~ 90-91 K). For the samples grown at the lowest temperature (720 ºC) the temperature dependence of J_c is shown in the inset of Figure 2. The increase of J_c in the Ag-assisted sample is effective in the whole range of temperatures.

SEM images confirm that Ag additives strongly reduce the disorder (Figures 3(a) to 3(e)). YBCO/Ag films grown at 720ºC, for instance, display some residual porosity, probably responsible of a slight reduction in J_c, but no a-axis nucleated crystals or disordered grains are observed, contrary to the YBCO films grown at the same temperature without Ag (Figure 3(b)).

Another important point to notice is the almost negligible presence of Ag in the final composition of the films. Only in the case of samples grown at 720 ºC some traces of Ag nanoparticles (diameter ~300nm) were identified (Figures 4(a)-(c)). In all other cases Ag was not detected by means of XRD or SEM/EDX analysis. This suggests that sublimation of Ag could occur during the YBCO formation process, a phenomena already observed in Ag nanoparticles [56].

The presence of undesired nucleation as, for example, a/b-axis grains, is easily detected by X-ray diffraction, μ-Raman spectroscopy and SEM images of the film surfaces [12, 53]. Figure 5 shows a comparison of the μ-Raman spectra of YBCO films grown with and without Ag additives at different temperatures, where the fraction of c-axis oriented grains, δ, has been quantified from the intensity ratio of the O(2,3) and the O(4) phonon modes [12, 57].

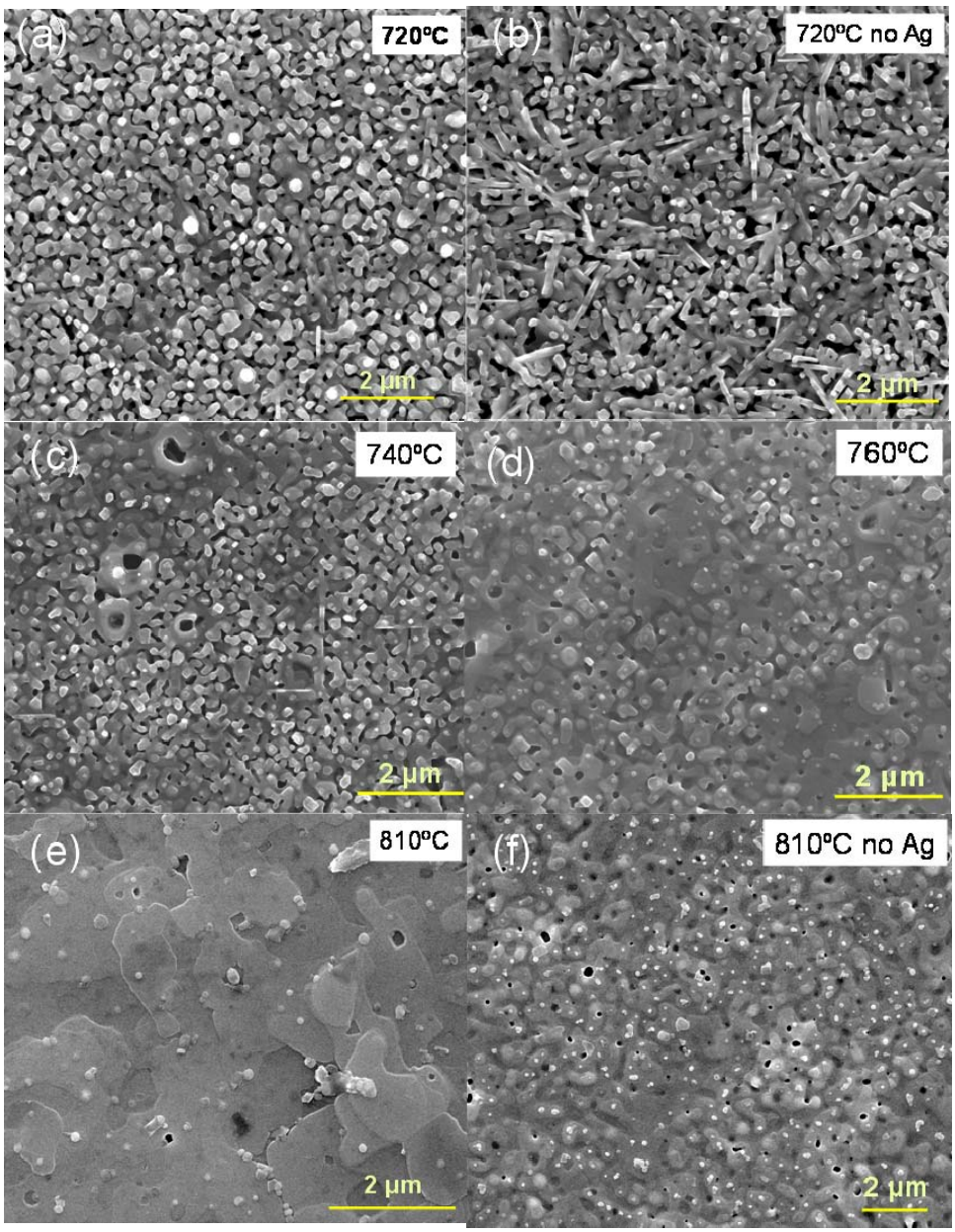

Fig. 3. (a) to (f) SEM images of YBCO film surface for samples grown on LAO substrates at different temperatures from 720ºC to 810 ºC including Ag or without Ag. (a) 720ºC with Ag; (b) 720ºC without Ag; (c) –(e) 740ºC, 760ºC and 810ºC with Ag; (f) 810ºC without Ag

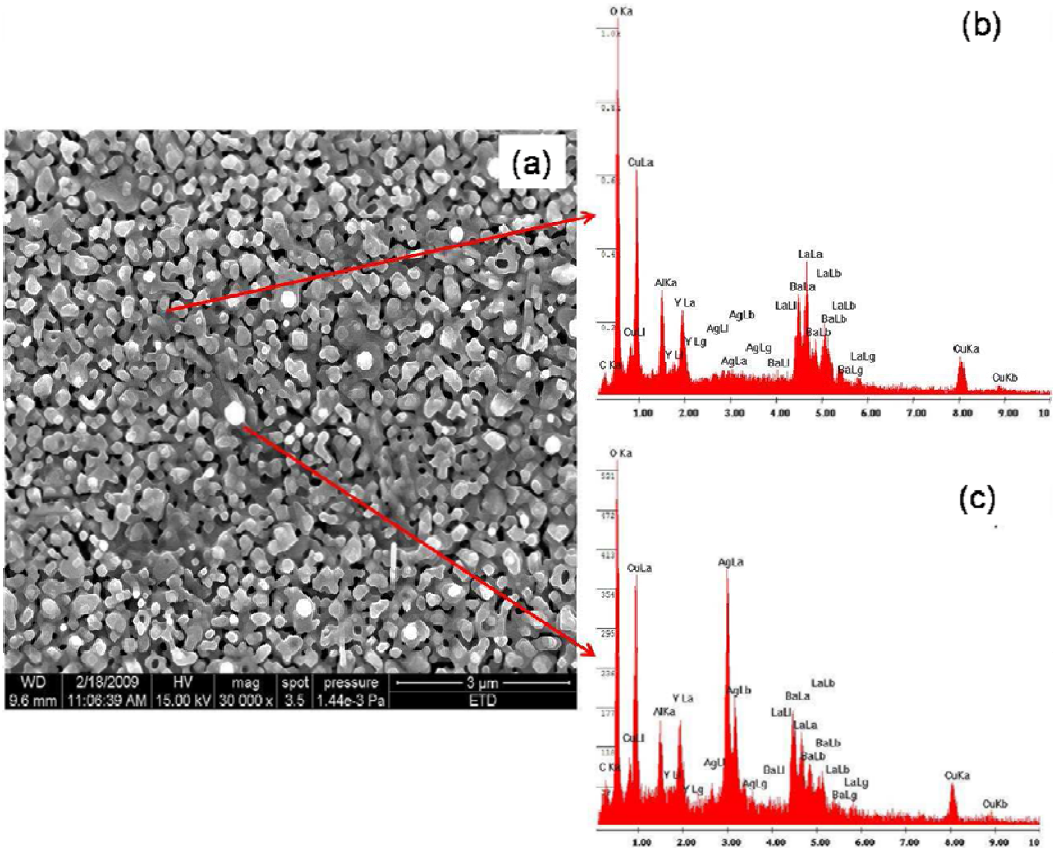

Fig. 4. (a) SEM and (b)-(c) EDX analysis of the surface of a YBCO/Ag film grown at 720ºC where Ag nanoparticles can be identified at the surface by EDX.

A different behaviour of nucleation with the presence of Ag is clearly observed. In the standard YBCO film there is a noticeable presence of non c-axis oriented grains when growth is performed at low temperature (δ~0.79 at 740ºC for instance) whereas they are almost absent in the Ag-assisted grown film at the same temperature (δ~0.95). As a consequence, no residual porosity, neither 90º grain boundaries exist in samples with Ag additives and thus, a higher critical current at self-field is achieved [12].

To understand this behaviour we should refer to the basic ideas concerning the nucleation mechanism of YBCO films, as described in the previous section.

In ex-situ grown YBCO films at P_t=1 atm c-axis nucleation is promoted when temperature is increased because $|\Delta\mu|$ in eq. (4) decreases when T is increased [12, 41, 42], i.e. supersaturation is decreased and ΔG*(001) is stabilized respect to ΔG*(100) (Figure 1) [38, 40, 43-46].

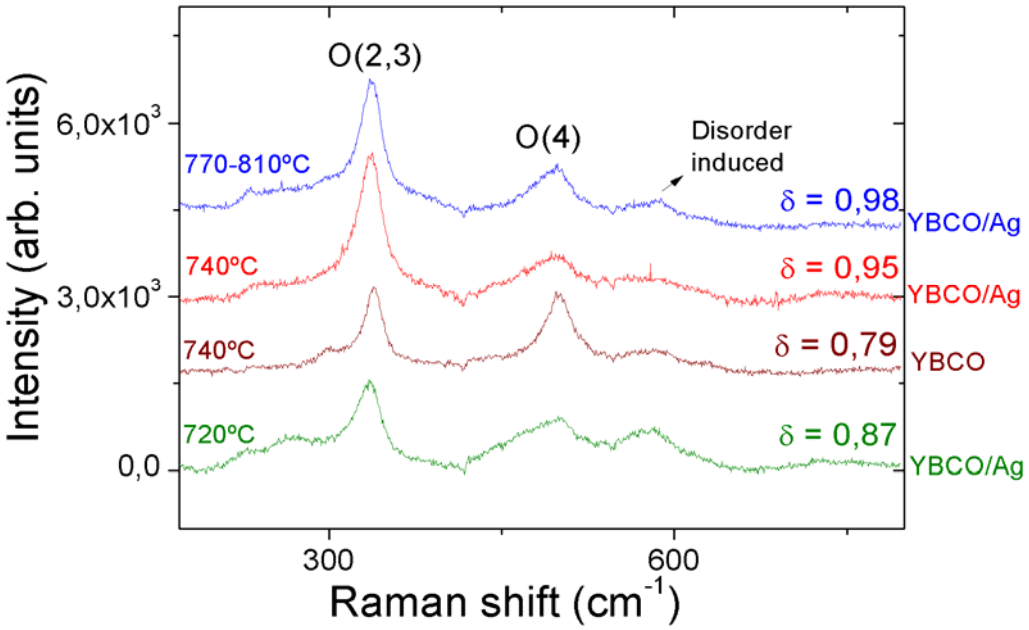

Fig. 5. (a) –(b) Comparison of μ-Raman spectra of YBCO films grown on CZO/YSZ substrates with and without Ag additives at different temperatures, as indicated. The calculated fraction of c-axis oriented crystals, δ, is also displayed.

When growth of YBCO/Ag composites is carried out, $\Delta\mu_o$ in eq. (4) is modified due to the slightly different thermodynamic properties of the YBCO/Ag system. The presence of Ag in the Y-Ba-Cu-O system remarkably reduces its peritectic temperature [58, 59]. As Δh_0 in eq. (4) is related to this peritectic temperature a decrease in the later one should lead to a lower Δh_o and thus to a diminution of $|\Delta\mu_0|$. As a consequence, the crossover temperature where c-axis nucleation becomes dominant ($\Delta G^*(001) < \Delta G^*(100)$) is thus shifted to a lower value than that observed in the standard YBCO system. This explains the absence of a/b-axis grains, even at 720ºC in the images of Figure 3(a), and the observed behaviour of J_c in the YBCO/Ag films. Also in agreement with this scenario is the fact that silver content has no influence on the final result. A similar behaviour was observed in samples with Ag additive from 2.5 mol % up to 20 mol %, suggesting that Ag only plays a role in facilitating the nuclei formation while then it sublimates. As a consequence the beneficial effects can be achieved with minor addition of Ag. The trend associated to Ag additives concerning nucleation has similarities to REBCO films where Yttrium is replaced by heavier rare earth ions, for

example, in YbBCO [40]. The presence of Yb also decreases the peritectic temperature and preferential c-axis nucleation is thus observed within an extended range of temperatures.

Another appealing feature of the Ag-assisted growth of YBCO films is that they present a much smoother surface morphology and a reduced residual porosity. Figures 3(e) and 3(f) compare SEM images with and without Ag additives, Figure 6(a) displays an AFM image of the surface of an YBCO/Ag film grown at 810 ºC and Figures 7(a) and 7(b) display FIB cross-section images of the films including Ag additives and a standard one.

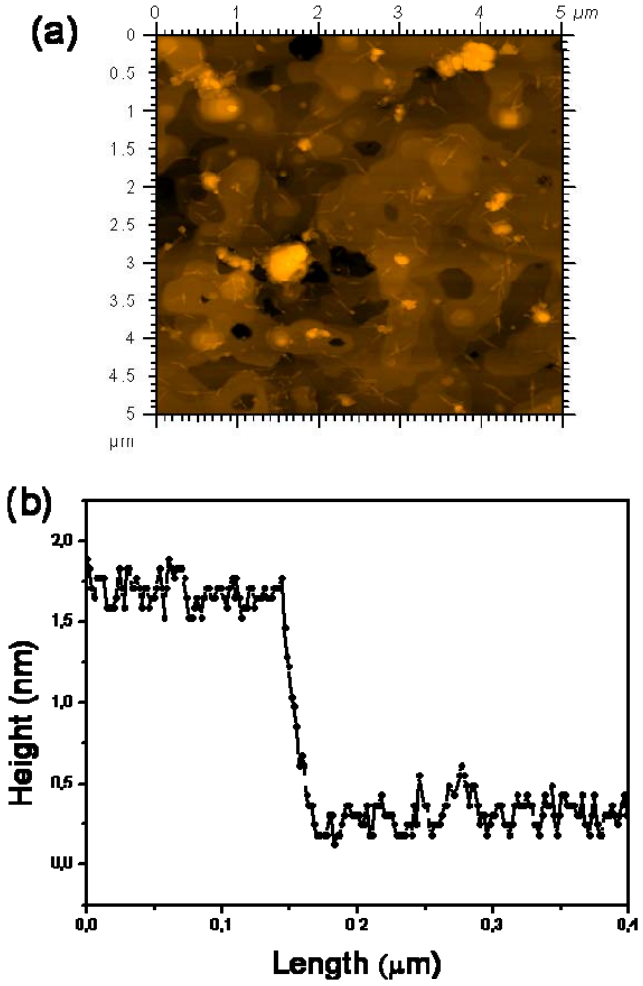

Fig. 6. (a) AFM surface image of a YBCO/Ag film grown at 810ºC on a LAO substrate; (b) line scan trough the AFM image in (a).

In the SEM picture we can observe the terraced morphology of the YBCO/Ag film surface with a remarkable absence of pores also confirmed in the cross-section FIB images.

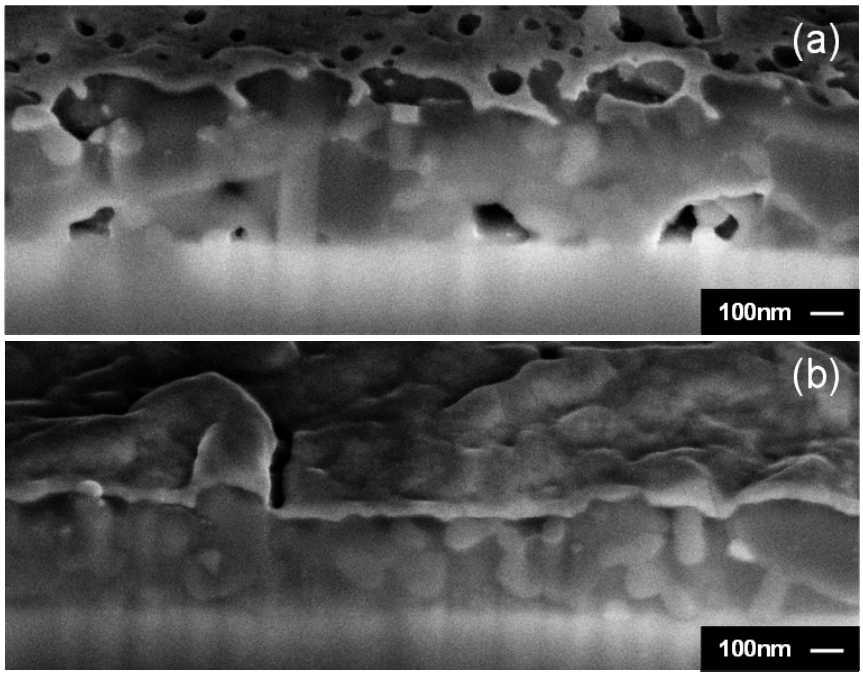

Fig. 7. Cross section FIB images of films quenched after reaching 810ºC (a) YBCO/Ag film; (b) a standard YBCO film.

The height of the observed terraces has been found to be as low as one unit-cell length, as demonstrated by the line profile in Figure 6(b) taken from the corresponding AFM image. Achieving atomically flat superconducting through Ag additions has been previously studied for in-situ grown films [60-64] where a change from 3D island growth mode to 2D layer-by-layer growth mode was claimed [65]. However, ex-situ film nucleation follows a Volmer-Weber mechanism and, after lateral grain growth and coalescence low angle grain boundaries remain which follow a zipping process leading to continuous reconstructed films [66, 67]. These processes are strongly influenced by atomic mobility and so they are enhanced at high reduced temperatures T/T_p, where T_p is the peritectic temperature. Thus, lowering T_p in YBCO/Ag should lead to an enhanced atomic mobility promoting faceting to reduce the surface energy [40, 44, 68]. As a consequence, when compared to pure YBCO films under the same growth

conditions, an enhanced planarity and reduced porosity is observed. A similar behaviour has been reported for in-situ grown YbBCO films [40].

V. MESOSCALE STRAIN AS A LIMITING FACTOR OF PERCOLATING CRITICAL CURRENTS

To study the GB zipping step in YBCO thin film growth, we followed the evolution with annealing time of microstructural features (intensity of Bragg peaks, microstrain) and the self-field J_c at 77 K. In situ measurements of electrical resistance of growing films were also carried out. A double step temperature annealing was applied (740ºC during t_1 and 770ºC during t_2) to separate nucleation and growth processes. PVD-CeO_2/YSZ single crystals were used in this investigation.

Figure 8(a) shows the normalized in-situ conductance of a YBCO film where the double temperature step is immediately visualized.

Assuming that the film was a conduction plate we can determine the corresponding thickness evolution. It was estimated that ~20% of the film (~ 50 nm) was grown after t_1=20 min at 740ºC while the rest of the film was grown at 770ºC up to a thickness 250±20 nm. The phase evolution during the growth process at 770ºC (t_2), after a nucleation time at 740ºC (t_1=20 min), was also followed through the time dependence (t_1+t_2) of the normalized intensity of X-ray diffraction patterns of YBCO ((005) peak) (Figure 8(b)). At the same time, the evolution of J_c at self-field and 77 K was also determined for these films. As it may be observed in Figure 8(b), while the formation of YBCO is completed at a total time of (30 ±5) min, a saturated J_c value is achieved much later (t_1+t_2 ~80 min). For instance, J_c is increased by a factor ~2.5 since the time when the full YBCO film was formed. Such an anomalous behavior requires a detailed microstructural investigation which was carried out by means of SEM and X-ray diffraction line broadening allowing to determine the microstrain [69, 70]. SEM images of films annealed during different times showed a slight improvement in the film porosity. Broadening of diffraction peaks occurs due to a limited size of coherent scattering volume and from the presence of inhomogeneous strain (r.m.s. strain). The first term is independent of diffraction order while the second is order dependent and so both terms can be separated through the angular dependence of line broadening. This

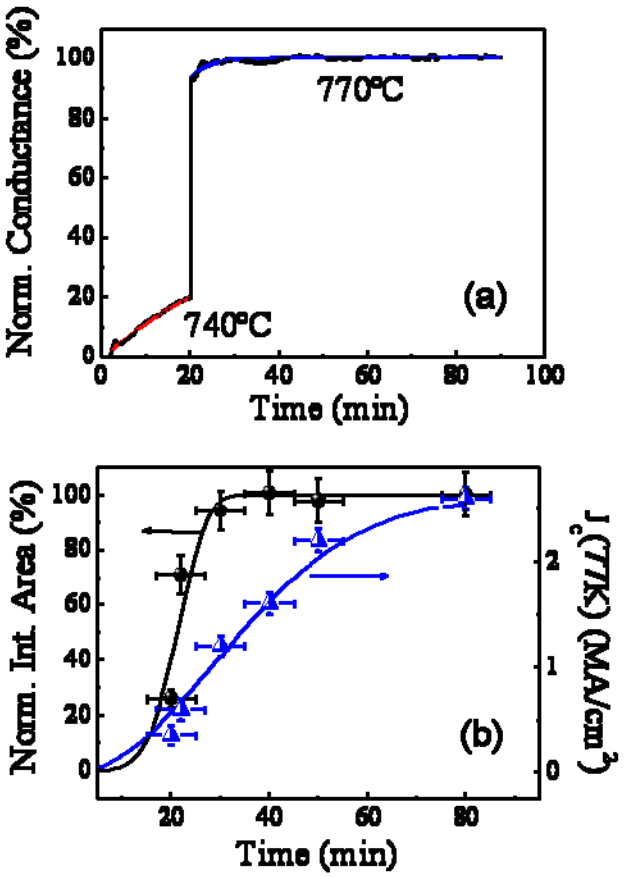

Fig. 8. (a) Normalized in-situ conductivity curve of the YBCO growth process on top of CeO_2/YSZ single crystal. A double temperature step was used to separate the nucleation and growth processes; (b) Time dependence of the normalized intensity of the (005) peak in the XRD patterns (circles) and critical current density, measured at 77 K in self-field (triangles).

can be done through the WH plot [70] which, even if it is a semiquantitative approach, it allows to track the evolution of the film microstructure. The WH plot relates the term associated to finite domain size with the microstrain through the following equation,

$$\beta_w^2 \cos^2\theta = \left(\frac{\lambda_{\alpha 1}}{L_\perp}\right) + 16\varepsilon^2 \sin^2\theta \qquad (7)$$

where β_w is the integral breadth of the Bragg peak after subtraction of the instrumental contribution, θ is the Bragg angle, $\lambda_{\alpha 1}$ = 1,5406 Å is the X-ray source radiation wavelength, $L_\perp$ is the size of the coherent volume perpendicular to the scattering vector and ε is the internal root-mean square strain parameter.

WH plots for the (00l) Bragg peaks of the YBCO films grown by the double step process, with different annealing times, are presented in Figure 9(a). Figure 9(b) shows that the microstrain is progressively reduced with annealing time and finally saturates.

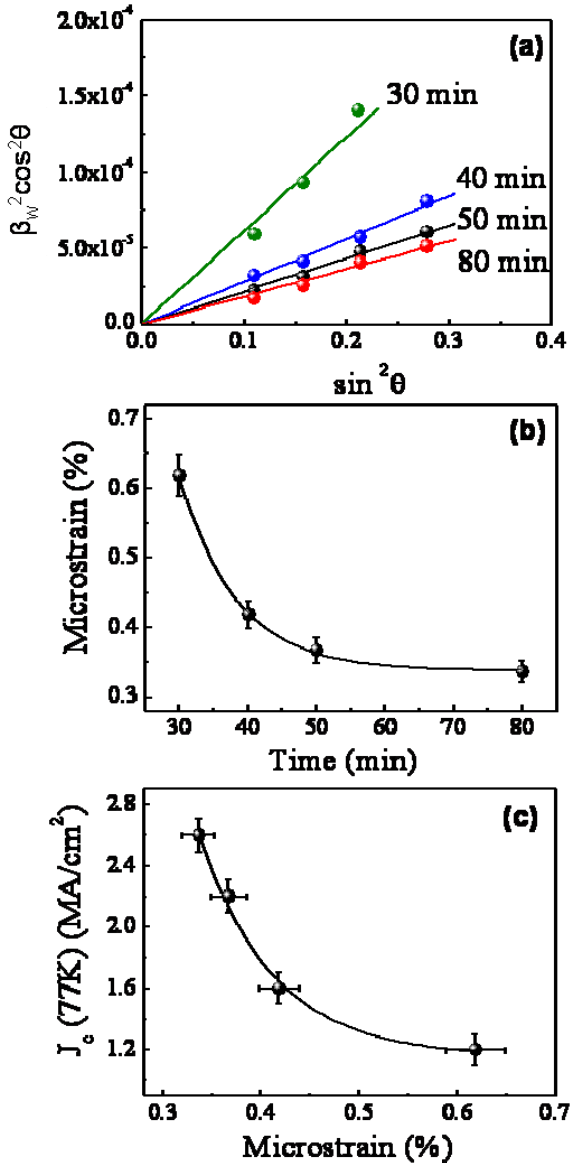

Fig. 9. (a) Williamson – Hall plots of YBCO/CeO_2/YSZ films grown during different times where it is visualized that the microstrain decreases as function of annealing time; (b) Time dependence of the microstrain in the films shown in (a); (c) Dependence of self-field J_c on the microstrain in the films annealed during different times.

The coherent domain size term $L_\perp$ was found to be consistent with the film thickness. A reduction with annealing time of the rms microstrain ε indicates that grain growth occurs through a boundary diffusion process, as it is typically observed in low temperature oxide ex-situ film growth [16, 67]. From the analysis of the annealing time

dependence of ε and J_c we come to an outstanding conclusion: there exists a strong adverse dependence of J_c on the microstrain in ex-situ grown YBCO films, as is shown in Figure 9(c). We observe that the relaxation of ε enhances J_c, thus demonstrating that the mesoscale strain generated during the grain zipping process introduces a weak-link behavior in the boundaries, contrary to nanoscale rms strain which enhances vortex pinning [71, 72]. This demonstrates that, even if the grain misorientation is very low (as it is confirmed by XRD texture analysis), the self-field percolating J_c can be strongly decreased by the strain accumulated there, similarly to the tensile strain generated by dislocations in low angle GBs [73].

To get further insight on the physical origin of the observed limitation in the percolating J_c we have used a very unique inductive technique, recently reported by Palau et al [31, 32] and already used in CSD-YBCO films and different sorts of CC's [32, 55, 74]. This methodology enables to determine the local critical current density J_c^G from a set of minor hysteresis loops and, simultaneously, the percolating current density J_c^{PERC} which extends through the whole film [31, 32, 75] thereby allowing to sort out the nanoscale and mesoscopic scale phenomena controlling J_c. We have applied this technique to the films having variable degrees of strain (see Figure 9(b)) and the results are reported in Figure 10.

For the YBCO film processed with t_1=20 min at 740ºC and t_2=0 min at 770°C, Figure 10(a) shows reversal branches of minor hysteresis loops obtained at 5 K after applying the maximum magnetic field indicated in the legend. The peak shift confirms the granular behavior of the film [24]. Similar measurements for other films show that the mesostrain relaxation runs in parallel to the disappearance of the granular behavior. Figure 10(b) shows that J_c^G values at 5K are independent of the total processing time, i.e. they are insensitive to ε. In contrast J_c^{PERC} increases until it reaches J_c^G . Thus, we conclude that the major mechanism reducing the J_c^{PERC} is actually the mesoscopic strain arising from the grain zipping process while the nanoscale phenomena influencing

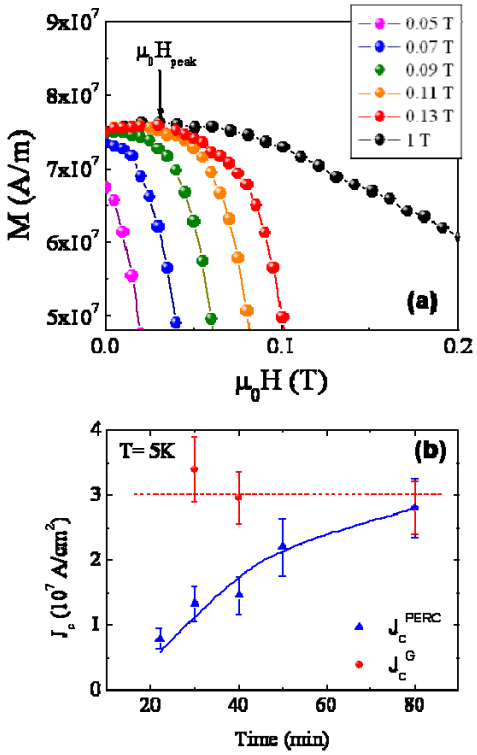

Fig. 10. (a) Detail around zero applied magnetic field of the reversed branches of minor hysteresis loops for a film grown during 0 min at 770ºC where the shift of the irreversible magnetization peak is visualized; (b) Dependence with growth time of the grain, J_c^G, and percolative, J_c^{PERC}, critical currents determined at 5 K.

vortex pinning and J_c^G are essentially not modified. The increase of J_c^{PERC} cannot be associated to a modification of the film porosity because then a strong reduction (~40 %) of the film normal state film conductance, at whatever temperature is measured, should be expected [75]. This would be in contradiction with our in-situ high temperature conductance measurements (see Fig. 8(a)) showing that during the time inducing mesostrain relaxation, the film conductance remains constant within ~ 5 %.

We have further investigated the relationship between mesostrain and J_c^{PERC} in different series of TFA-YBCO thin films grown on CZO/YSZ single crystals where the growth temperature was modified in the range 735ºC-810ºC and we have indeed confirmed that, as a general trend, samples displaying enhanced J_c^{PERC} (in the range 1-4 MA/cm^2 at 77 K) have reduced mesostrain values (ε~ 0.12-0.27 %). The tendency is that growing at higher temperatures reduces the mesostrain, in accordance with our interpretation that atomic mobility is required to heal out the GB disorder. However, more systematic analysis of well defined processes is required to fully clarify the mechanisms controlling the persistence of mesostrain in ex-situ grown films.

A novel scenario concerning the physical origin of the correlation between strain and the superconducting order parameter has been recently introduced, based on the bond contraction pairing (BCP) model, first introduced by Deutscher and de Gennes [76]. The BCP model shows that pair formation stems from a delicate balance in energy between the paired state of two holes localized on opposite sides of an oxygen atom and the state of free holes with energy related to the top of the valence band. The pair breaking energy 2Δ can be then written as

$$2\Delta = 4\frac{(t_{CuO})^2}{U} - 8t_0 \qquad (8)$$

where t_{CuO} is the transfer integral between a d orbital (Cu) and a p orbital (O), U is the on-site Coulomb repulsion and $4t_o$ is the half bandwidth. In the BCP model, the pairs are formed when the first term in eq. (8) overcomes the second one, so that Δ is positive. Because t_{CuO} is strongly sensitive to the Cu-O bond length, a tensile strain of about 1% may inhibit pairing; thus, the universal weak-link behavior observed in HTS and pnictides can be explained by the tensile strain generated by the GB dislocations [29, 73, 77]. This model has been also proposed to be at the basis of a novel vortex pinning mechanism recently discovered in CSD prepared YBCO nanocomposites [71, 78]. Noteworthy, however, the phenomenological relationship we have demonstrated here for the first time to exist between the mesostrain and J_c^{PERC} certainly requires further experimental and theoretical analysis. Particularly it will be needed to scrutinize quantitatively at the nanoscale the coupling between structure and pair energy condensation. Also it will be useful to extend the XRD mesostrain analysis, performed here with symmetrical Bragg peaks and thus only being sensitive to the ε_{zz} strain component, to asymmetric peaks which should provide additional information about the in-plane ε_{xx} strain component [29]. This analysis would certainly help to understand the complex behavior of grain boundaries in ex-situ grown CC's.

VI. SUMMARY

We have first reviewed the state of the art of nucleation phenomena in ex-situ grown YBCO films having BaF_2 as a precursor, i.e. the so called TFA-YBCO route. It have been highlighted the general trends of this complex phenomenon. A proper consideration of the nucleation conditions, separately from those optimizing the growth rate, is found to be required. We have also presented a novel approach allowing to

widen the conditions leading to c-axis oriented epitaxial growth of ex-situ grown YBCO thin films. We have shown that the addition of Ag to the precursor solution results in an enhanced stability of c-axis nuclei allowing the use of a larger window of processing temperatures. This study also proves that Ag-assisted growth of thin films leads to smoother surfaces with a reduced porosity.

On the other hand, we have investigated the relationship between percolating J_c and the mesostrain generated during the grain boundary zipping process following island coalescence. We have shown that mesoscopic strain generated during ex-situ growth of TFA-YBCO superconducting films is adversely correlated with the percolating J_c, even in low angle GBs. Mesostrain is found to be enhanced when annealing times are too short or performed at temperatures too low. The intragrain J_c of these non-optimally processed films is demonstrated to be constant and so the nanoscale structure should be essentially not modified. A physical origin of the adverse correlation between mesostrain and superconducting properties is suggested. This is based on the bond contraction pair model which predicts that in-plane tensile strain prevents pair formation in YBCO and hence leads to a weak link behavior associated to the low angle grain boundaries.

ACKNOWLEDGEMENTS

The authors would like to thank MICINN (MAT2008-01022), Consolider NANOSELECT (CSD2007-00041), Generalitat de Catalunya (2009 SGR 770 and Xarmae) and EU (HIPERCHEM and NESPA).

REFERENCES

[1] A. P. Malozemoff, S. Fleshler, M. Rupich, C. Thieme, X. Li, W. Zhang, A. Otto, J. Maguire, D. Folts, J. Yuan, H. P. Kraemer, W. Schmidt, M. Wohlfart, and H. W. Neumueller, Superconductor Science & Technology 21 (2008) 034005.

[2] X. Obradors, T. Puig, A. Pomar, F. Sandiumenge, N. Mestres, M. Coll, A. Cavallaro, N. Roma, J. Gazquez, J. C. Gonzalez, O. Castano, J. Gutierrez, A. Palau, K. Zalamova, S. Morlens, A. Hassini, M. Gibert, S. Ricart, J. M. Moreto, S. Pinol, D. Isfort, and J. Bock, Superconductor Science & Technology 19 (2006) S13.

[3] T. Izumi, M. Yoshizumi, J. Matsuda, K. Nakaoka, Y. Kitoh, Y. Sutoh, T. Nakanishi, A. Nakal, K. Suzuki, Y. Yamada, A. Yajima, T. Saitoh, and Y. Shiohara, Physica C-Superconductivity and Its Applications 463 (2007) 510.

[4] O. Castano, A. Cavallaro, A. Palau, J. C. Gonzalez, M. Rossell, T. Puig, F. Sandiumenge, N. Mestres, S. Pinol, A. Pomar, and X. Obradors, Superconductor Science & Technology 16 (2003) 45.

[5] T. Araki and I. Hirabayashi, Superconductor Science & Technology 16 (2003) R71.

[6] A. Gupta, R. Jagannathan, E. I. Cooper, E. A. Giess, J. I. Landman, and B. W. Hussey, Applied Physics Letters 52 (1988) 2077.

[7] M. Vilardell, X. Granados, S. Ricart, R. Cobas, M. Arjona, T. Puig, X. Obradors, S. C. Hopkins, B. A. Glowacki, J. Bennewitz, M. Falter, and M. Baecker, Journal of Imaging Science and Technology 55 (2011) 040304.

[8] M. W. Rupich, D. T. Verebelyi, W. Zhang, T. Kodenkandath, and X. P. Li, Mrs Bulletin 29 (2004) 572.

[9] T. G. Holesinger, Q. Jia, B. Maiorov, L. Civale, P. C. Dowden, and B. J. Gibbons, Advanced Materials 19 (2007) 1917.

[10] K. Zalamova, N. Roma, A. Pomar, S. Morlens, T. Puig, J. Gazquez, A. E. Carrillo, F. Sandiumenge, S. Ricart, N. Mestres, and X. Obradors, Chemistry of Materials 18 (2006) 5897.

[11] A. Llordes, K. Zalamova, S. Ricart, A. Palau, A. Pomar, T. Puig, A. Hardy, M. K. Van Bael, and X. Obradors, Chemistry of Materials 22 (2010) 1686.

[12] T. Puig, J. C. Gonzalez, A. Pomar, N. Mestres, O. Castano, M. Coll, J. Gazquez, F. Sandiumenge, S. Pinol, and X. Obradors, Superconductor Science & Technology 18 (2005) 1141.

[13] H. Chen, K. Zalamova, A. Pomar, X. Granados, T. Puig, and X. Obradors, Superconductor Science & Technology 23 (2010) 034005.

[14] N. Mori, K. Tada, K. Yamada, R. Teranishi, and M. Mukaida, Physica C-Superconductivity and Its Applications 468 (2008) 1537.

[15] N. Mori, K. Yoshida, Y. Miyanaga, K. Yamada, R. Teranishi, and M. Mukaida, Physica C-Superconductivity and Its Applications 469 (2009) 1341.[16] V. F. Solovyov, K. Develos-Bagarinao, and D. Nykypanchuk, Physical Review B 80 (2009) 104102.

[17] V. F. Solovyov, H. J. Wiesmann, Q. Li, D. O. Welch, and M. Suenaga, Journal of Applied Physics 99 (2006) 013902.

[18] V. F. Solovyov, H. J. Wiesmann, and M. Suenaga, Ieee Transactions on Applied Superconductivity 15 (2005) 2739.

[19] Y. L. Xu, Z. Q. Qian, Z. Y. Xu, P. He, M. Massey, and R. Bhattacharya, Ieee Transactions on Applied Superconductivity 19 (2009) 3127.

[20] R. Feenstra, F. A. List, X. Li, M. W. Rupich, D. J. Miller, V. A. Maroni, Y. Zhang, J. R. Thompson, and D. K. Christen, Ieee Transactions on Applied Superconductivity 19 (2009) 3131.

[21] H. Chen, K. Zalamova, A. Pomar, X. Granados, T. Puig, and X. Obradors, Journal of Materials Research 25 (2010) 2371.

[22] D. M. Feldmann, D. C. Larbalestier, R. Feenstra, A. A. Gapud, J. D. Budai, T. G. Holesinger, and P. N. Arendt, Applied Physics Letters 83 (2003) 3951.

[23] A. Palau, T. Puig, X. Obradors, R. Feenstra, and A. A. Gapud, Applied Physics Letters 88 (2006) 122502.
[24] A. Palau, T. Puig, X. Obradors, R. Feenstra, A. A. Gapud, E. D. Specht, D. M. Feldmann, and T. G. Holesinger, Applied Physics Letters 88 (2006) 132508.
[25] D. M. Feldmann, T. G. Holesinger, R. Feenstra, C. Cantoni, W. Zhang, M. Rupich, X. Li, J. H. Durrell, A. Gurevich, and D. C. Larbalestier, Journal of Applied Physics 102 (2007) 083912.
[26] H. Hilgenkamp and J. Mannhart, Reviews of Modern Physics 74 (2002) 485.
[27] S. Graser, P. J. Hirschfeld, T. Kopp, R. Gutser, B. M. Andersen, and J. Mannhart, Nature Physics 6 (2010) 609.
[28] Y.A. Soh, G. Aeppli, N. D. Mathur, and M. G. Blamire, Phys. Rev. B63 (2000) 020402.
[29] G. Deutscher, Applied Physics Letters 96 (2010) 122502.
[30] N. Roma, S. Morlens, S. Ricart, K. Zalamova, J. M. Moreto, A. Pomar, T. Puig, and X. Obradors, Superconductor Science & Technology 19 (2006) 521.
[31] A. Palau, T. Puig, X. Obradors, E. Pardo, C. Navau, A. Sanchez, A. Usoskin, H. C. Freyhardt, L. Fernandez, B. Holzapfel, and R. Feenstra, Applied Physics Letters 84 (2004) 230.
[32] A. Palau, T. Puig, X. Obradors, and C. Jooss, Physical Review B 75 (2007) 054517.
[33] R. Feenstra, T. B. Lindemer, J. D. Budai, and M. D. Galloway, Journal of Applied Physics 69 (1991) 6569.
[34] V. F. Solovyov, H. J. Wiesmann, and M. Suenaga, Superconductor Science & Technology 18 (2005) 239.
[35] J. Gazquez, F. Sandiumenge, M. Coll, A. Pomar, N. Mestres, T. Puig, X. Obradors, Y. Kihn, M. J. Casanove, and C. Ballesteros, Chemistry of Materials 18 (2006) 6211.
[36] M. Gibert, A. Garcia, T. Puig, and X. Obradors, Physical Review B 82 (2010)
[37] M. Gibert, P. Abellan, A. Benedetti, T. Puig, F. Sandiumenge, A. Garcia, and X. Obradors, Small 6 (2010) 2716.
[38] F. M. Granozio, M. Salluzzo, U. S. di Uccio, I. Maggio-Aprile, and O. Fischer, Physical Review B 61 (2000) 756.
[39] M. Gibert, P. Abellan, L. Martinez, E. Roman, A. Crespi, F. Sandiumenge, T. Puig, and X. Obradors, Cryst. Eng. Comm 13 (2011) 6719.
[40] Y. Ichino, K. Sudoh, K. Miyachi, Y. Yoshida, and Y. Takai, IEEE Transactions on Applied Superconductivity 13 (2003) 2735.
[41] T. Endo, K. Yoshii, S. Iwasaki, H. Kohmoto, H. Saratani, S. Shiomi, M. Matsui, and Y. Kurosaki, Superconductor Science & Technology 16 (2003) 110.
[42] Y. Q. Cai, X. Yao, and Y. J. Lai, Journal of Applied Physics 99 (2006) 113909.
[43] F. M. Granozio and U. S. diUccio, Journal of Alloys and Compounds 251 (1997) 56.
[44] F. M. Granozio and U. S. diUccio, Journal of Crystal Growth 174 (1997) 409.
[45] C. Y. Tang, Y. Y. Chen, W. Li, L. J. Sun, X. Yao, and M. Jirsa, Crystal Growth & Design 10 (2010) 575.
[46] C. Klemenz, I. Utke, and H. J. Scheel, Journal of Crystal Growth 204 (1999) 62.
[47] V. A. Shchukin and D. Bimberg, Reviews of Modern Physics 71 (1999) 1125.
[48] V. F. Solovyov, D. Abraimov, D. Miller, Q. Li, and H. Wiesmann, Journal of Applied Physics 105 (2009) 113927.
[49] M. Coll, J. Gazquez, R. Huehne, B. Holzapfel, Y. Morilla, J. Garcia-Lopez, A. Pomar, F. Sandiumenge, T. Puig, and X. Obradors, Journal of Materials Research 24 (2009) 1446.
[50] V. R. Vlad, K. Zalamova, M. Coll, A. Pomar, A. Palau, J. Gutierrez, T. Puig, X. Obradors, and A. Usoskin, Ieee Transactions on Applied Superconductivity 19 (2009) 3212.
[51] M. Yoshizumi, I. Seleznev, and M. J. Cima, Physica C-Superconductivity and Its Applications 403 (2004) 191.
[52] D. E. Wesolowski, M. Yoshizumi, and M. J. Cima, Physica C-Superconductivity and Its Applications 450 (2006) 76.
[53] O. Castano, A. Cavallaro, A. Palau, J. C. Gonzalez, M. Rosell, T. Puig, S. Pinol, N. Mestres, F. Sandiumenge, A. Pomar, and X. Obradors, Ieee Transactions on Applied Superconductivity 13 (2003) 2504.

[54] A. Pomar, V. R. Vlad, A. Llordes, A. Palau, J. Gutierrez, S. Ricart, T. Puig, X. Obradors, and A. Usoskin, Ieee Transactions on Applied Superconductivity 19 (2009) 3258.
[55] A. Pomar, J. Gutierrez, A. Palau, T. Puig, and X. Obradors, Physical Review B 73 (2006) 214522.
[56] Y. Ding, F. R. Fan, Z. Q. Tian, and Z. L. Wang, Small 5 (2009) 2812.
[57] J. C. Gonzalez, N. Mestres, T. Puig, J. Gazquez, F. Sandiumenge, X. Obradors, A. Usoskin, C. Jooss, H. C. Freyhardt, and R. Feenstra, Physical Review B 70 (2004) 094525.
[58] J. L. Macmanus Driscoll, J. C. Bravman, and R. B. Beyers, Physica C-Superconductivity and Its Applications 241 (1995) 401.
[59] U. Wiesner, G. Krabbes, M. Ueltzen, C. Magerkurth, J. Plewa, and H. Altenburg, Physica C-Superconductivity and Its Applications 294 (1998) 17.
[60] P. Selvam, E. W. Seibt, D. Kumar, R. Pinto, and P. R. Apte, Applied Physics Letters 71 (1997) 137.
[61] D. Kumar, M. Sharon, P. R. Apte, R. Pinto, S. P. Pai, S. C. Purandare, C. P. Dsouza, L. C. Gupta, and R. Vijayaraghavan, Journal of Applied Physics 76 (1994) 1349.
[62] R. Pinto, P. R. Apte, S. P. Pai, and D. Kumar, Physica C-Superconductivity and Its Applications 207 (1993) 13.
[63] R. Kalyanaraman, S. Oktyabrsky, and J. Narayan, Journal of Applied Physics 85 (1999) 6636.
[64] R. Pinto, N. Goyal, S. P. Pai, P. R. Apte, L. C. Gupta, and R. Vijayaraghavan, Journal of Applied Physics 73 (1993) 5105.
[65] Y. Yoshida, K. Sudoh, Y. Ichino, I. Hirabayashi, and Y. Takai, Ieee Transactions on Applied Superconductivity 13 (2003) 2785.
[66] J. A. Floro, E. Chason, R. C. Cammarata, and D. J. Srolovitz, Mrs Bulletin 27 (2002) 19.
[67] V. F. Solovyov, K. Develos-Bagarinao, Q. Li, J. Qing, and J. Zhou, Superconductor Science & Technology 23 (2010) 014008.
[68] M. Coll, J. Gazquez, A. Pomar, T. Puig, F. Sandiumenge, and X. Obradors, Physical Review B 73 (2006)
[69] H. P. Klug and L. E. Alexander, X-Ray Diffraction Procedures For Polycrystalline and Amorphous Materials, John Wiley and Sons, Inc., 1974.
[70] G. K. Williamson and W. H. Hall, Acta Metallurgica 1 (1953) 22.
[71] J. Gutiérrez, A. Llordés, J. Gazquez, M. Gibert, N. Romá, S. Ricart, A. Pomar, F. Sandiumenge, N. Mestres, T. Puig, and X. Obradors, Nature Materials 6 (2007) 367.
[72] T. Puig, J. Gutierrez, A. Pomar, A. Llordes, J. Gazquez, S. Ricart, F. Sandiumenge, and X. Obradors, Superconductor Science & Technology 21 (2008) 034008.
[73] D. C. van der Laan, T. J. Haugan, and P. N. Barnes, Physical Review Letters 103 (2009) 027005.
[74] R. Feenstra, J. W. Sinclair, J. R. Thompson, and D. K. Christen, Superconductor Science & Technology 24 (2011)
[75] E. Bartolomé, F. Gömory, X. Granados, T. Puig, and X. Obradors, Superconductor Science & Technology 20 (2007) 895.
[76] G. Deutscher and P.-G. de Gennes, Comptes Rendus Physique 8 (2007) 937.
[77] A. Gurevich and E. A. Pashitskii, Physical Review B 57 (1998) 13878.
[78] A. Llordés, A. Palau, J. Gázquez, M. Coll , V. R. Vlad, A. Pomar, J.Arbiol, R.Guzmán, S. Ye , V. Rouco, F. Sandiumenge, S. Ricart, T. Puig, M. Varela, D.Chateigner, J. Vanacken, J. Gutiérrez, V. Moshchalkov, G. Deutscher, C. Magen, and X.Obradors, to be published